Advances in Science and Technology
ISSN: 1662-0356, Vol. 51, pp 81-89
doi:10.4028/www.scientific.net/AST.51.81

Online: 2006-10-01

Carbon-based and other nanostructures obtained via cluster-assembling: a view combining electron spectroscopies and nanospectroscopies

L. Gavioli[1,a] and M. Sancrotti[1,2,b]

[1]Dipartimento di Matematica e Fisica, Università Cattolica del Sacro Cuore,

Via dei Musei 41, I-25121 Brescia, Italy

[2]Laboratorio Nazionale TASC CNR-INFM, AREA Science Park,

Strada Statale 14, Km. 163 Basovizza, I-34012, Trieste, Italy

[a]gavioli@dmf.unicatt.it

[b]sancrotti@tasc.infm.it

Keywords: cluster-assembling, carbon and titanium nanoclusters, electronic structure.

Abstract. This work will provide an overview of recent experiments devoted to study the nature and properties of materials obtained *in situ* via cluster-assembling, by using supersonic cluster beam deposition. This technique has proved to be a powerful tool for assembling nanostructured materials with tailored physical properties, in particular for: 1) carbon-based clusters deposited *in situ* on appropriate substrates in Ultra High Vacuum compatible conditions; 2) a micro-structured pattern based on pristine carbon-based dots and then promoted to the formation of SiC via *in situ* thermal annealing; 3) thermo-chemically doped nanostructured TiO_2, revealing the possibility to control the band gap of this material. The electronic structure of the systems has been studied combining a wide variety of experimental methods, including valence-band and core-level photoemission, Electron Energy Loss Spectroscopy, Scanning Auger Spectroscopy, Atomic Force Microscopy.

Introduction

Cluster beam deposition (CBD) has opened a number of possibilities for synthesizing innovative materials, characterized by different physical and functional properties [1,2]. These properties are subtly determined by the mass distribution of the precursor aggregates, cluster-surface interaction, and the degree of cluster coalescence [3]. A variety of systems have been explored so far, in which the geometrical structure can be tailored on a wide range of lengths, up to the mesoscale [1,2]. Research has been pursued on nanostructured covalent materials such as carbon, silicon, silicon carbide [4-6] and on transition metal oxides [7,8] such as titanium dioxide [8].

For cluster-assembled carbon it is possible to control the film morphology and structure on the nano- and mesoscale [4-6,9-11]. The cluster-assembled carbon films show different structural and functional properties compared to carbon films assembled atom by atom [11-13]. The realization of a ultrahigh vacuum (UHV) compatible supersonic cluster beam deposition source (SCBD) [14-16], that can be attached to different experimental stations to perform a wide variety of experimental investigations, makes it possible to investigate the early stages of cluster deposition in ultraclean conditions. This allows to address fundamental issues such as the role played by the clusters at the submonolayer regime, where the interaction with the substrate is a clue point in determining the further evolution of thin-film growth and its resulting features (roughness, texture development, electronic transport, etc.).

Among nanostructured transition metal oxides, titanium dioxide has been one of the most studied due to its versatility for applications in photocatalysis, optics, gas sensing etc. [7]. Previous extensive investigations on such systems has not completely understood the interplay between nanostructure, stoichiometry, catalytic behavior and crystalline structure [17], in particular on the issue of photocatalytic splitting of water by solar irradiation [18,19]. Again, the possibility of fabricating the specimens *in situ* to avoid any undesired contamination makes the interpretation of any experimental response (photoemission, optical, vibrational, etc.) more straightforward and actually reliable.

The paper is organized in sections: the experimental section is briefly describing the cluster source and the basic experimental conditions, while the scientific topics are introduced in more details in each separate section, followed by a brief summary of the experimental techniques used for each experiment, and by the topic discussion.

Experimental

Cluster deposition is performed at room temperature (RT) by means of a UHV-compatible source, which is described in detail in Ref. [14]. The system is based on a pulsed microplasma cluster source [15], placed in the first of three differentially pumped UHV vacuum chambers. The clusters nucleation takes place in a small ceramic cavity by condensation of carbon atoms in presence of an inert buffer gas (helium). Atoms are sputtered from the appropriate target by the helium atoms ionized during an intense discharge between two electrodes. The aggregates exit the source through a nozzle in a highly collimated molecular supersonic beam with a narrow velocity distribution. The kinetic energy of the clusters is less than 0.4 eV/at., so the deposition on a substrate does not lead to fragmentation or implantation phenomena. The mass of the clusters follows a log-normal distribution law and ranges from a few to about 2500 atoms. The equivalent thickness mentioned in the following has been deduced from the deposition rate measured with a quartz microbalance placed in the source third chamber. Since the clusters are not mass selected, in the calculation for the thickness determination we referred to the mean cluster size (900 atoms/cluster).

X-ray photoemission spectroscopy (XPS), ultra-violet photoemission spectroscopy (UPS), Auger spectroscopy and electron energy-loss spectroscopy (EELS) have been performed using conventional sources [20,21]. Scanning electron microscopy (SEM) and spatially resolved Auger spectroscopy (SR-AES) characterizations have been performed using a FEI electron-gun with a nominal beam diameter of 20 nm. The SEM images are acquired collecting both the secondaries and backscattered electrons, while auger integrated spectra are obtained with a cylindrical sector analyzer [21].

Carbon and Sic

Cluster-assembled covalent materials such as carbon and silicon show substantial differences from the corresponding amorphous systems [4,5]. The case of silicon carbide produced by SCBD is even more challenging, since different types of ordering, bonding, and reactivity in cluster-assembled SiC is observed, depending on the precursors used (silicon-carbon clusters or Si-doped heterofullerenes [6,22]). Alternative routes for production of nanostructured SiC are thermal decomposition of C_{60} or hydrocarbons deposited on silicon [23-25], or annealing of carbon clusters with linear, planar, and cage structures [4]. The comprehension of the carbide production process from carbon clusters precursors deposited by SCBD, demands appropriate investigation of the temperature-dependent evolution of their physical properties.

Fig. 1 shows the electron energy-loss spectrum of a 30 nm thick cluster-assembled film, deposited onto Si(100)-(2x1) at 300 K under UHV conditions, compared to EELS of a C_{60} multilayer, polycrystalline (pc) graphite, sputtered polycrystalline graphite, and sputtered C_{60} multilayer specimens, measured in the same experimental conditions.

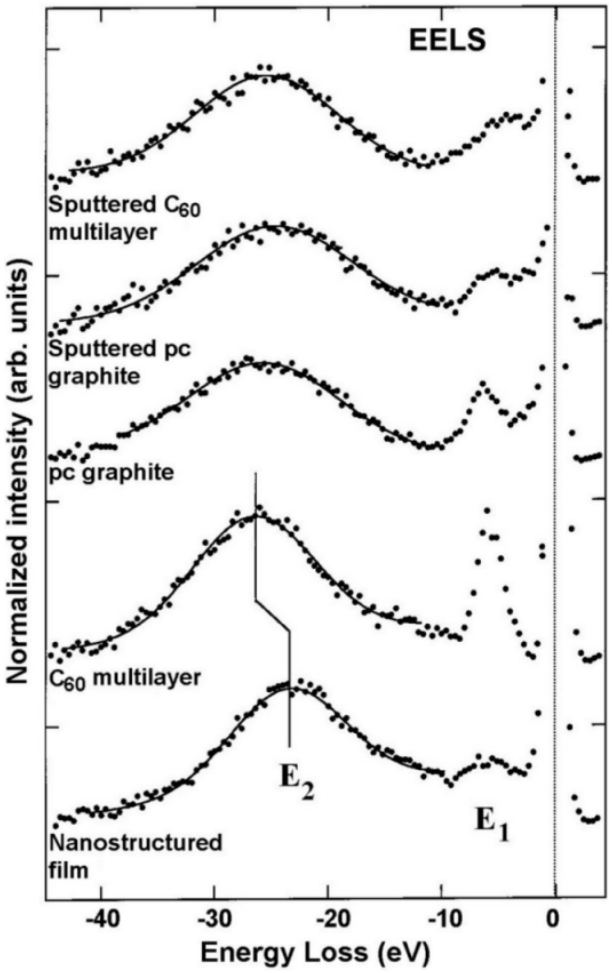

Figure 1. Electron energy loss spectra taken on different carbon-based systems, with primary beam energy of 1 keV in reflection geometry (angle of incidence 20°). The spectra are normalized at the elastic peak intensity. From each spectrum a linear background has been subtracted in order to allow an easy comparison of the main structures of the spectra. The (σ+π)-related profile (E_2) was fitted by a Gaussian line and the results of the fitting procedure are superimposed to the spectra.

The two loss features characterizing all spectra represent the collective excitations of valence electrons present in the sp_2 bonded system. The first peak (E_1) arises from $\pi \rightarrow \pi^*$ transitions, and the second broader peak (E_2) is associated with the (σ+π) plasmon loss. The intensity and shape of E_1 observed in the EELS spectrum of the nanostructured sample is similar to that of the sputtered layers, indicating a reduced graphitic character and reduced order [20]. The (σ+π) plasmon loss peak of the nanostructured film occurs at an energy lower than in pc graphite and in the C_{60} multilayer. This energy is an intermediate value between the extreme values found for two distinct cluster sizes of nanostructured films [26]. This can be explained as an effect of the focalizing nozzle, acting like a low-band pass filter for clusters leaving the source [16,27]. The expected effect on cluster size distribution is to obtain an intermediate average size with respect to the cases reported in Ref. [26], as is indeed confirmed by the energy of the plasmon loss. The different C bonding configurations, observed by C 1s XPS spectra taken on nanostructured layers, are similar to those observed on amorphous carbon films [28], and do not change upon layer thickness variation [20,28].

The thermal-induced effects on a thick nanostructured carbon film are shown in Fig. 2. The C 1s spectrum is very similar to that of the as-deposited film up to 700 °C, while a new peak appears at lower binding energy at 800 °C. This feature signals the formation of silicon carbide that is likely to initiate at the silicon-cluster film interface [20]. The formation of SiC takes places in a similar way as for C_{60} and hydrocarbons on silicon substrates [23-25]: out diffusion of Si atoms from substrate is followed by the chemical reaction with carbon. In the present case, the SiC feature appears already at 700 °C, a temperature lower compared to SiC formation using C_{60} as precursor [20]. This

can be explained by considering the highly defected structure of clusters, which would favor carburization reaction at lower temperatures compared to fullerenes.

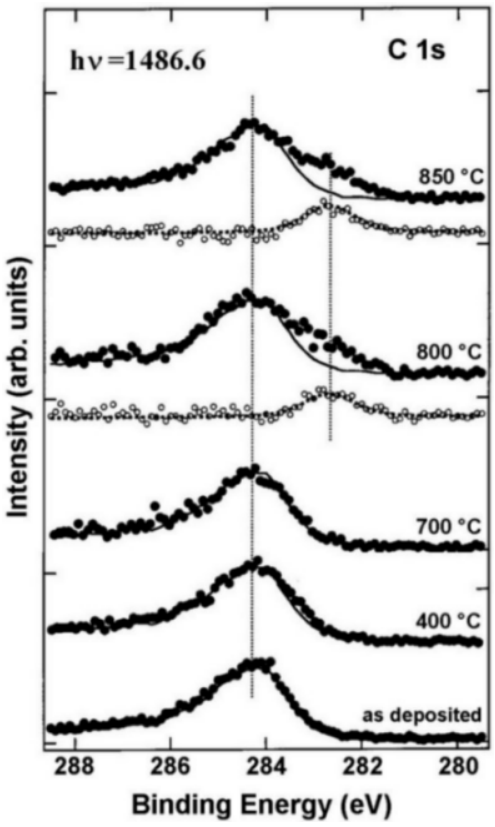

Figure 2. Carbon 1s XPS spectra taken after annealing a 30 ML-thick nanostructured film at selected temperatures. Each spectrum has been analyzed by subtracting the spectrum measured on the as-deposited film. The difference spectrum (open circle) has been fitted (dotted line) by a single component located at 282.7 eV binding energy. The component is a combination of Gaussian and Lorentzian line shapes, accounting for the instrumental and lifetime broadening, respectively.

SiC microstructures

Cluster-assembled Carbon dots arrays have been fabricated by supersonic cluster beam deposition on a Si(100) substrate, sonicated in acetone before deposition to preserve the surface native oxide, and using as a stencil mask a commercial electron grid for transmission electron microscopy [29]. After deposition the sample has been transferred for characterization into the UHV apparatus equipped with SEM and SR-AES. The sample was directly annealed for about one hour at selected temperatures ranging from RT to 1100 °C. The typical working conditions are beam voltage 15 kV and beam current 2 nA. Si $L_{23}VV$ and C KVV integrated spectra were measured both on the top of the dots and in the regions between the dots. AFM measurements were also performed on the samples before and after the process of thermal heating, using a commercial AFM (Digital Instruments Multimode IIIa), operated in air in both tapping and contact mode.

Part of the pattern of ns-carbon dots is shown in the SEM images of Fig. 3a and b, measured at RT and after annealing at 1100 °C, respectively. A set of SR-AES spectra, taken from selected points of the pattern, is presented in Fig. 1(c) and (d). This allows to analyze the chemical composition of the dots and of the regions between the dots. At RT the only detected signal on the dot is due to the presence of C, while in the regions between the dots, both C and Si signals are observed (Fig. 1(c)). Note that the observed contrast in the SEM image of Fig. 1(a) can be explained considering the difference in the average atomic number Z between dots and substrate,

since at 15 KV beam energy the contribution from the secondary electrons is, to a first approximation, similar for the two materials [21].

After annealing at 1100 °C the contrast of the SEM images (Fig. 1(b)) is suddenly inverted. Moreover, the SR-AES measurements show the presence of C and Si signals both coming from the dots and from the regions between the dots, but with differences in the C KVV Auger line shape between RT and after annealing at 1100 °C.

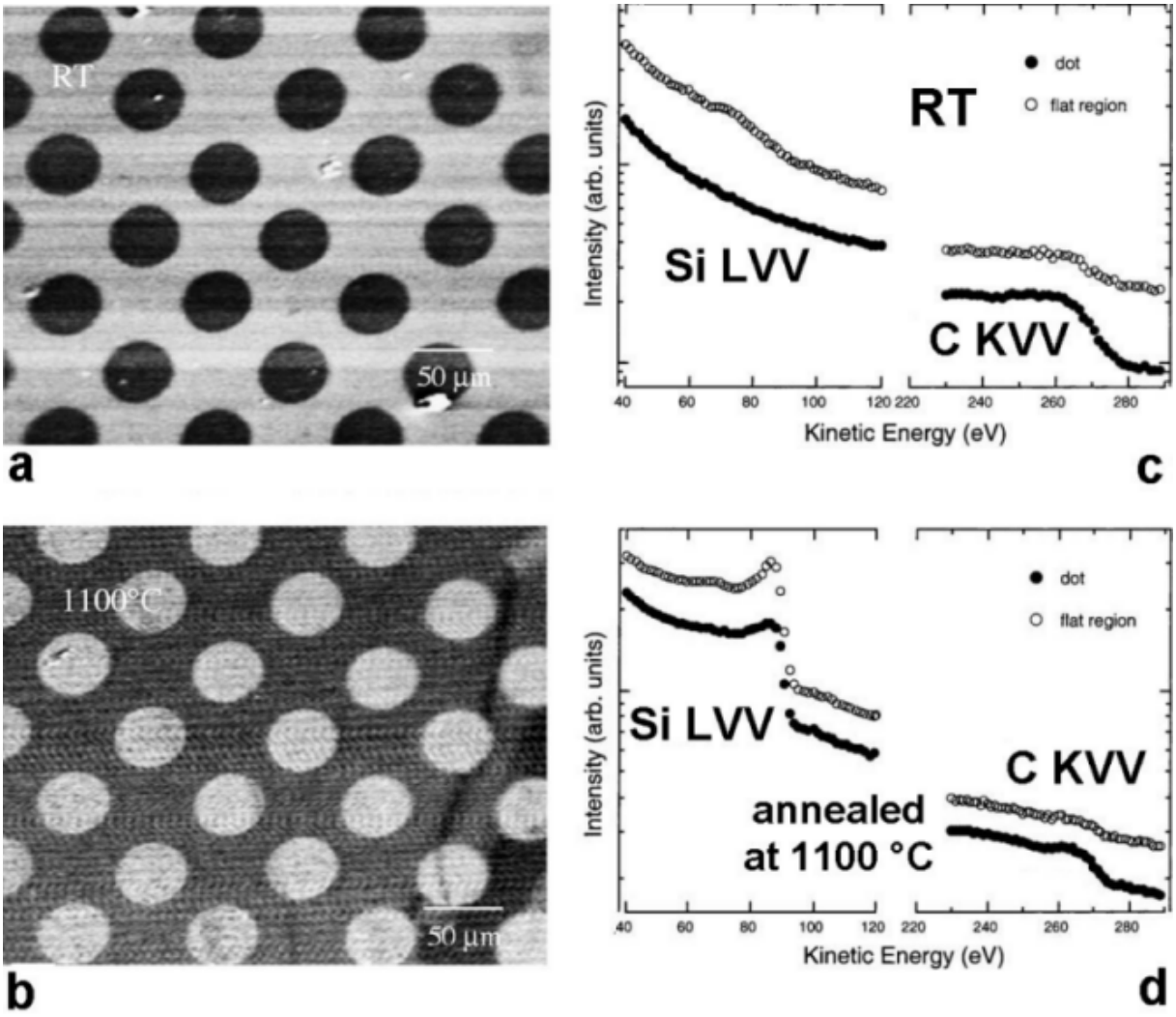

Figure 3. SEM images of a portion of the pattern of ns-carbon dots measured (a) at RT and (b) after annealing at 1100 °C. SR-AES spectra taken from selected points of the sample (c) at RT and (d) after annealing at 1100 °C.

Detailed analysis of normalized spectra [21] shows that carbon bonding at RT is graphitic [20], while after annealing at 1100 °C both on the flat regions and on the dots the C KVV line shape changes in agreement with the formation of a carbidic bonding with Si [30]. At the same time, the Si LVV signal from the dot changes with respect to the spectrum measured from the flat region, in particular the shoulder at ~70 eV is shifted at lower kinetic energy. The line shape becomes typical of Si–C bonding [31], while the signal from the flat regions is primarily due to Si–Si bonding [32].

The results of the thermal treatment is the following: the dots are characterized by the formation of carbidic bonds, while the regions between them expose prevalently the clean silicon surface, with the presence of isolated carbon clusters bound to the Si substrate atoms through the formation of carbidic bonds.

The inverted contrast in the SEM images after annealing at 1100 °C (Fig. 3b) is not consistent with a compositional contrast, rather with the case where secondary electron signals can vary strongly with very small changes in composition [33]. It was observed indeed, that the expected atomic number contrast between the silicon (white) and the silicon carbide (dark) is observed when only backscattered electrons are detected, while the corresponding secondary plus backscattered electron image shows reversed contrast between the silicon (black) and silicon carbide (white) [33].

AFM characterization of dots (not shown) reveals the presence of small pits (lateral dimension of few hundreds of nanometers and up to 200 nm deep) all around the dots. The presence of pits has a fundamental role in the carburization of the material forming the dots [34]. At the very first stage, the silicon atoms at the dot/silicon substrate interface react with the carbon clusters forming a thin SiC layer. Annealing the sample sustains the carburization reaction by enhancing the silicon diffusion from the substrate toward the nanostructured carbon overlayer. A thicker SiC layer is thus formed. Since the Si diffusion coefficient through bulk SiC is very low [35], the formation of pits at the silicon–SiC interface, may represents a preferred diffusion channel, providing Si atoms for the reaction with the carbon overlayers [35]. It is very important to note that even at this high temperature the lateral resolution of the dots defined by the stencil mask is maintained in the SiC structure and no degradation of the pattern is observed.

TiO_2 nanostructured films

The interest in TiO_2 as strategic material for environmental photocatalysis was raised by the observation of photocatalytic splitting of water on rutile TiO_2 [36]. The photocatalytic effect in a solid state catalysts takes places when an exciton can interact with molecules close to the catalysts surface. For common polymorphic TiO^2, the wide optical gap (about 3.0 eV [37]) hampers the exciton creation by the visible solar spectrum. Moreover, the catalytic activity is affected by the catalyst nanostructure [8]. Therefore, several strategies were proposed to narrow the TiO2 energy gap, in particular, by doping with metallic and non metallic atoms.

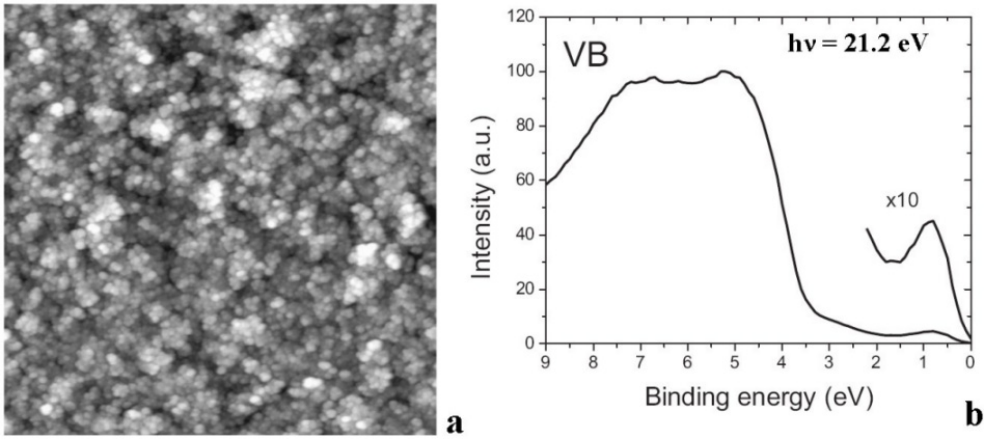

Figure 4. a) Surface morphology of nanostructured TiO_2 film obtained by AFM (image size 2 x 2 μm^2). b) UPS spectrum of the film shown in a). Note the magnification of the peak located at 0.8 eV below Fermi level.

The thermal instability shown by transition metal doped TiO_2 [38] stimulated the effort of employing non metallic atoms. Investigation of gap narrowing by carbon doping of microcrystalline TiO_2 indicated a considerable inhomogenity of doping concentration and Ti oxidation [39].

The present approach is based on a nanostructured system obtained by supersonic cluster beam deposition under high vacuum conditions [8]. The film thickness is ranging from 500 to 1000 nm, with TiO_2 nanocrystals size of about 15 nm (Fig. 4a). UPS spectroscopy of the film presents a large density of states at 0.8 eV below the Fermi level (Fig. 4b), indicating a considerable presence of $Ti3^+$ point defects, due to oxygen vacancies. These defects act as surface chemisorption sites and, together with the large porosity of the material, suggest that annealing in air can enable carbon incorporation into the film by thermal decomposition of carbon-containing adsorbed molecules.

Thermal treatment at 1000 °C of the nanostructured film in air induces a grain growth to about 75 nm in size. The element concentration obtained by XPS are 17 % for C, 20 % for Ti and 42 % of Oxigen related, with no detectable signals of Ti-bonded carbon [8]. The optical response of the annealed film is shown in Fig. 5a, compared to the transmission coefficient of the as-deposited film. The annealed sample presents a rigid shift of the adsorption edge towards 630 nm, suggesting that the film has undergone a substitutional process in the TiO_2 lattice [8,40], incorporating carbon as a dopant. The shift is accompanied by a variation of the optical gap from 3.36 eV in the as-deposited film, to 2.06 eV in the annealed film. Following the evolution of the gap as a function of annealing temperature (Fig. 5b) suggest the importance of the carbon doping as the mechanism causing the gap narrowing. The gap remains basically constant up to 800 °C, with a sudden drop below 3 eV occurring at 900 °C. Such behavior is indicating that carbon diffusion and subsequent doping is taking place. The importance of the nanostructured film as the enabling factor for the carbothermal doping is confirmed by the absence of gap variation for a TiO2 film with the same stoichiometry but with a compact structure.

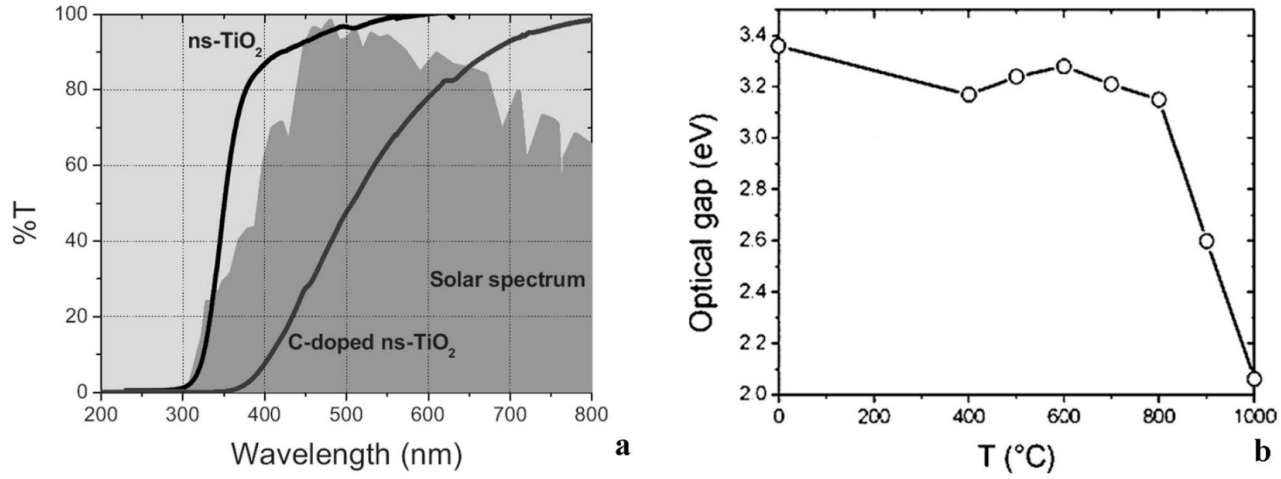

Figure 5. a) Ultra violet–vis transmittance spectra for carbon doped and as-deposited nanostructured TiO_2 films. The solar spectrum at the sea level is reported in darker gray. b) Optical gap as a function of annealing temperature.

Conclusions

The unique possibility of exploring *in situ* nanostructured films obtained by supersonic cluster beam deposition has been reviewed for some cases. The work performed on SiC and TiO_2 suggests that the investigation of produced film without external contamination is providing a powerful tool to understand many processes involved in the determination of the film properties.

Aknowledgements

The works presented were partially supported by Fondazione Cariplo and by the FIRB project Carbon-based nanostructures and microstructures. The nanospectroscopy facility in Brescia was funded by INFM under the Strumentazione Avanzata program.

References

[1] P. Milani and S. Iannotta: Cluster Beam Synthesis of Nanostructured Materials (Springer-Verlag, Berlin, 1999)

[2] C. Binns, Surf. Sci. Rep. Vol. 44 (2001), p. 1

[3] P. Jensen, Rev. Mod. Phys. Vol. 71 (1999), p. 1695

[4] D. Donadio, L. Colombo, P. Milani, G. Benedek, Phys. Rev. Lett. Vol. 83 (1999), p. 776

[5] P. Melinon, P. Keghelian, B. Prevel, A. Perez, G. Guiraud, J. LeBrusq, J. Lermé, M. Pellarin, M. Broyer, J. Chem. Phys. Vol. 107 (1997), p. 10278

[6] P. Melinon, P. Keghelian, A. Perez, C. Ray, J. Lermé, M. Pellarin, M. Broyer, M. Beudeulle, B. Champagnon, J. L. Rousset, Phys. Rev. B Vol. 58 (1998), p. 16 481

[7] R.W. Siegel, in Physics of New Materials, (Springer-Verlag, Berlin 1998)

[8] E. Barborini, A.M. Conti, I. Kholmanov, P. Piseri, A. Podestà, P. Milani, C. Cepek, O. Sakho, R. Macovez, M. Sancrotti, Adv. Mater. Vol 17 (2005), p. 1842

[9] F. Siviero, E. Barborini, C. Boragno, R. Buzio, E. Gnecco, C. Lenardi, P. Piseri, S. Vinati, U. Valbusa, P. Milani, Surf. Sci. Vol. 513 (2002), p. 381

[10] P. Milani, P. Piseri, E. Barborini, A. Podestà, C. Lenardi, J. Vac. Sci. Technol. A Vol. 19 (2001), p. 2025

[11] C. S. Casari, A. Li Bassi, C. E. Bottani, E. Barborini, P. Piseri, A.Podestà, P. Milani, Phys. Rev. B Vol. 64 (2001), p. 085417

[12] L. Diederich, E. Barborini, P. Piseri, A. Podesta´, P. Milani, A. Schneuvly, R. Gallay, Appl. Phys. Lett. Vol. 75 (1999), p. 2662

[13] A. C. Ferrari, B. S. Satyanarayana, J. Robertson, W. I. Milne, E. Barborini, P. Piseri, P. Milani, Europhys. Lett. Vol. 46 (1999), p. 245

[14] E. Barborini, F. Siviero, S. Vinati, C. Lenardi, P. Piseri, P.Milani, Rev. Sci. Instrum. Vol 73 (2002), p. 2060

[15] E. Barborini, P. Piseri, P. Milani, J. Phys. D Vol 32 (1999), p. L105

[16] P. Piseri, A. Podestà, E. Barborini, P. Milani, Rev. Sci. Instrum. Vol 72 (2001), p. 2261

[17] D. Zhao, J. Feng, Q. Huo, N. Melosh, G.H. Fredrickson, B.F. Chmelka, G.D. Stucky, Science Vol 279 (1998), p. 548

[18] S. Inagaki, S. Guan, T. Ohsuna, O. Terasaki, Nature Vol 304 (2992), p. 416

[19] G. Temtsin, t. Afera, S. Bittner, G.A. Ozin, J. Mater. Chem. Vol 11 (2001), p. 3202

[20] E. Magnano, C. Cepek, M. Sancrotti, F. Siviero, S. Vinati, C. Lenardi, P. Piseri, E. Barborini, P. Milani, Phys. Rev. B Vol. 67 (2003), p. 125414

[21] E. Magnano, M. Padovani, V. Spreafico, M. Sancrotti, A. Podestà, E. Barborini, P. Piseri, P. Milani, Surf. Sci. Vol 544 (2003), p. L709

[22] P. Melinon, X. Blase, P. Keghelian, A. Perez, C. Ray, M. Pellarin, M. Broyer, B. Champagnon, Phys. Rev. B Vol. 65 (2002), p. 125321

[23] C. Cepek, P. Schiavuta, M. Sancrotti, M. Pedio, Phys. Rev. B Vol. 60 (1999), p. 2068

[24] K. Sakamoto, T. Suzuki, M. Harada, T. Wakita, S. Suto, Phys. Rev. B Vol. 57 (1998), p. 9003

[25] G. Dufour, F. Rochet, F. C. Stedile, Ch. Poncey, M. De Crescenzi, R. Gunnella, M. Froment, Phys. Rev. B Vol. 56 **(**1997**)**, p. 4266

[26] E. Riedo, E. Magnano, S. Rubini, M. Sancrotti, E. Barborini, P. Piseri, P. Milani, Sol. State Commun. Vol. 116 (2000), p. 287

[27] H. Vahedi Tafreshi, G. Benedek, P. Piseri, S. Vinati, E. Barborini, P. Milani, Aerosol. Sci. Technol. Vol. 36 (2002), p. 593

[28] J. Diaz, G. Paolicelli, S. Ferrer, F. Comin, Phys. Rev. B Vol. 54 (1996), p. 8064

[29] E. Barborini, P. Piseri, A. Podestà, P. Milani, Appl. Phys. Lett. Vol. 77 (2000), p. 1059

[30] A.J. Nelson, A.R. Mason, A.B. Swartzlander, L.L. Kazmerski, N. Saxena, C.M. Fortmann, T.W.F. Russell, J. Vac. Sci. Technol. A Vol. 15 (1990), p. 1538

[31] A. Gölz, G. Lucovsky, K. Koh, D. Wolfe, H. Niimi, H. Kurz, J. Vac. Sci. Technol. B Vol. 15 (1997), p. 1097

[32] S.M. Durbin, T. Gog, Phys. Rev. Lett. Vol. 63 (1989), p. 1304

[33] J.I. Goldstein, D.E. Newbury, P. Echlin, D.C. Joy, C. Fiori, E. Lifshin: Scanning Electron Microscopy and X-ray Microanalysis (Plenum Press, New York, 1997)

[34] K. Volz, S. Schreiber, J.W. Gerlach, W. Reiber, B. Rauschenbach, B. Stritzker, W. Assmann, W. Ensinger, Mat. Sci. Eng. A Vol. 289 (2000), p. 255

[35] D. Chen, R. Workman, D. Sarid, Surf. Sci. Vol. 344 (1995), p. 23

[36] A. Fujishima, K. Honda, Nature Vol. 238 (1972), p. 37

[37] A. Bendavid, P.J. Martin, A. Jamting, H. Takikawa, Thin Sol. Films Vol 355-356 (1999), p. 6

[38] T. Umebayashi, T. Yamaki, S. Yamamoto, A. Miyashita, S. Tanaka, T. Sumita, K. Asai, J. appl. Phys. Vol. 93 (2003) p. 5156

[39] S.U.M. Khan, M. Al-Shahry, W.B. Ingler, Jr., Science Vol. 297 (2002), p. 2243

[40] A.P. Wight, M.E. Davis, Chem. Rev Vol. 102 (2002), p. 3589